Pump-Probe Microscopy in a Sagnac Interferometer

JONAH M. THEISEN,[1] ERIK M. GRUMSTRUP[1,2,*]

[1]*Department of Chemistry and Biochemistry, Montana State University, Bozeman, MT, USA 59717*
[2]*Materials Science and Engineering Program, Montana State University, Bozeman, MT, USA 59717*
*erik.grumstrup@montana.edu

Received XX Month XXXX; revised XX Month, XXXX; accepted XX Month XXXX; posted XX Month XXXX (Doc. ID XXXXX); published XX Month XXXX

An interferometric pump-probe microscope with two counterpropagating probe beams is developed and characterized. Application of the technique to a porphyrin derivative thin film shows the technique is sensitive to variations in local film morphology that are undetectable with conventional pump-probe techniques. Analysis of the material response shows that the technique enhances signal levels measuring transient changes in the optical constants, limited by the asymmetry of the probe beam beamsplitter. The technique also provides the ability to distinguish contributions to the overall pump-probe response from changes to the real and imaginary components of the optical constants.

Pump-probe microscopy is a nonlinear optical technique that integrates spectroscopy and microscopy elements to enable high spatial and temporal resolution probes of complex systems. While the technique has found primary relevance in the characterization of electronic and photonic materials, it has shown to be a powerful tool for label-free biological imaging and even art conservation[1-4]. Generally, the technique relies on the detection of small changes in the optical constants of a sample, induced by a pump pulse, which is often temporally separated. The small ($\Delta I/I \sim 10^{-3} - 10^{-5}$) pump-probe signals are generally resolved via lock-in detection or by direct subtraction of "pump-on" and "pump-off" signals.

Because of the technique's intrinsically small signal sizes, numerous approaches aimed at maximizing signal to noise ratios (S/N) have been pursued. Simply increasing pump power is often limited by sample degradation and nonlinear dynamics that complicate spectroscopic interpretation[3, 5]. High laser repetition rates can help overcome fluence limitations by signal averaging lower energy pulses[2, 3], but high repetition rates can be incompatible with the frame rates of multipixel detectors necessary for broadband or widefield imaging[6, 7]. The integration of lock-in cameras overcomes some widefield imaging limitations and S/N levels that approach single element detection has been achieved in some cases[6, 8]. Others have implemented interferometric or holographic detection approaches to improve S/N levels[5, 7, 9].

Here, we implement a simple interferometric microscope for enhancing pump-probe signal magnitude by means of a Sagnac interferometer. Sagnac interferometers are common path interferometers which have been exploited in a variety of applications including rotational rate measurements[10], gravitational-wave detection[11], and in nonlinear spectroscopies[12-14]. For microscopy applications, modified Sagnac interferometers have been implemented to resolve transient picosecond to nanosecond thermal and acoustic responses in microscale materials[15]. This implementation is particularly useful for materials spectroscopy because it is insensitive to sample roughness, enables arbitrary polarization control of pump and probe beams, and can be readily modified to accommodate variable excited state lifetimes. Moreover, as we show below, the phase sensitivity of the technique provides the ability to disentangle changes to the real and imaginary components of the optical constants[16].

Figure 1 shows a schematic of the interferometric pump-probe (IPP) microscope and a pulse timing sequence. The Sagnac interferometer is comprised of the two counterpropagating probe pulses centered at 800 nm, derived from a cube beamsplitter (Newport 05BC17MB.2). The sample is placed asymmetrically in the interferometer, such that the counterclockwise (CCW) pulse precedes the clockwise (CW) pulse by $\Delta t_{CW} + \Delta t_{CCW} = 1.9\,ns$ (Fig. 1B). Because the probe path is delayed relative to the fixed pump with a translation stage (not shown in Fig. 1A), Δt_{CW} and Δt_{CCW} both change with the pump-probe delay. Thus the interferometer length constrains the maximum pump-probe delay time[17]. The CW probe, transmitted through the beamsplitter, is coupled collinearly with the 400 nm pump beam via a dichroic beamsplitter. The CW and CCW beams are focused and collected by a pair of objectives (Olympus, x40, NA=0.6) with correction collars adjusted to account for the air/sample interface (Obj. 1) or glass slide/sample interface (Obj. 2).

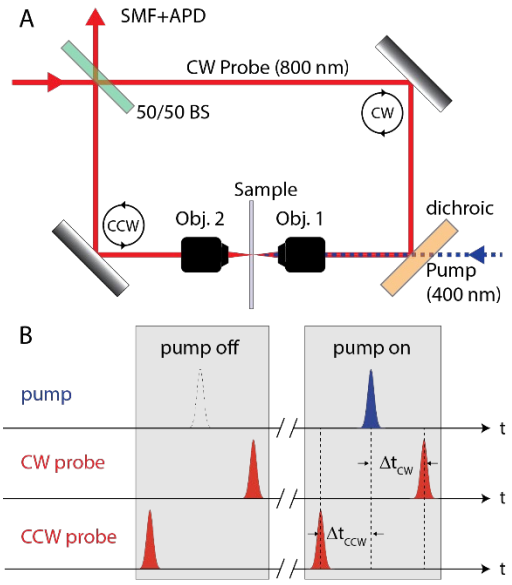

Fig. 1. (A) Schematic of the Sagnac interferometer design for IPP measurements. BS: beamsplitter; CW: clockwise probe path; CCW: counterclockwise probe path; Obj: microscope objective. SMF+APD: single mode fiber coupled avalanche photodiode. (B) Pulse sequence for IPP collection. The probe is delayed relative to the pump with a mechanical delay stage before the BS of the Sagnac interferometer.

The dark output of the interferometer is passed through a 750 nm longpass filter, coupled into a single mode fiber using a 75 mm lens, and detected on a silicon avalanche photodiode (Hamamatsu C10508-01). The photodiode signal is sent to a two-output resistive splitter (Mini-Circuits ZFRSC-2050+), with one output sent to a lock-in amplifier (Stanford Research SR830, to measure ΔI) and the other output sent to a data acquisition card (to measure I). For comparative non-interferometric measurements, the beamsplitter was vertically tilted to steer the CCW beam out of alignment. We found that matching objectives before and after the sample and spatial mode filtering via the single mode fiber were essential to achieve good destructive interference between the two arms[18]. Careful alignment of the counterpropagating beams resulted in ~94% intensity cancellation at the output of the interferometer, relative to the single CW arm.

The output of the interferometer is given by equation 1:

$$I_{out} = \left|\left(\frac{1}{2}+\delta\right)E_{in}\exp[\phi_{cw}] - \left(\frac{1}{2}-\delta\right)E_{in}\exp[\phi_{ccw}]\right|^2 \text{, Error! Bookmark not defined.} \quad (1)$$

where δ parameterizes the beamsplitter asymmetry, E_{in} is the complex field amplitude, and $\phi_{CW/CCW}$ are the complex phases associated with propagation through the sample. For the CW arm, the accumulated phase is perturbed by the presence of the pump, Eq. 2:

$$\phi_{cw} = -[(\kappa + \Delta\kappa(\tau_{CW})) + i(n + \Delta n(\tau_{CW}))]k_0 l, \quad (2)$$

where κ and $\Delta\kappa(\tau_{CW})$ parameterize the steady state and pump-induced extinction coefficient, k_0 is the free space k-vector, n and $\Delta n(\tau_{CW})$ are the steady state and pump-induced change to the refractive index, and l is the sample path length.

The detected IPP signal intensity is given by (see supporting information - SI) Eq. 3:

$$S_{IPP} = \frac{\Delta I_{IPP}}{I_{IPP}} \approx \frac{-k_0 l}{2\delta}\Delta\kappa + \frac{l^2 k_0^2}{16\delta^2}\Delta n^2, \quad (3)$$

where we've dropped the explicit τ_{CW}-dependence of $\Delta\kappa$ and Δn, and assumed that $|\delta| \ll 1$, $|\Delta\kappa| \ll 1$, and $|\Delta n| \ll 1$. Comparison to the "standard" pump probe signal,

$$\textbf{Error! Bookmark not defined.}\ S_{PP} = \frac{\Delta I_{PP}}{I_{PP}} = -2\Delta\kappa\, k_0\, l\,, \quad (4)$$

shows that interferometric detection provides an absorptive signal enhancement of $1/4\delta$. For the beamsplitter used in our apparatus, $\delta = 0.069$ (SI), implying a 3.6-fold signal enhancement for IPP detection. Beamsplitters with smaller values of δ will provide greater signal enhancements, however in practice the interferometer leakage ($\propto 4\delta^2$) will always be finite due to beamsplitter spectral flatness deviation, pulse front asymmetry from beam inversion paired with mirror non-uniformities, polarization rotation, and other non-idealities of the interferometer. Moreover, the leakage serves as a local oscillator for the signal field, and so optimization of signal to noise levels will require adjustment of the leakage depending on signal magnitude and measurement noise[12, 14].

The second term in Eq. 3 depends on Δn^2. Because the signal intensity scales quadratically with Δn, power-dependent measurements could in principle provide a means to disentangle contributions from the real and imaginary components of the optical constants. However, for typical values $\Delta\kappa \sim 10^{-4}$ and $\Delta n \sim 10^{-4}$, and for a sample path length, $l \sim 5\times10^{-7}\ m$, the (absorptive) first term is more than 100-fold larger than the (dispersive) second term with an asymmetry of $\delta = 0.069$. Moreover, as we discuss below, the primary contribution of Δn to S_{IPP} is not through the photoinduced phase shift expressed in Eq. 4, but rather through reflective gain/loss at the air-sample interface. Nevertheless, for well-balanced interferometers ($\delta \lesssim 10^{-3}$), contributions to S_{IPP} quadratic in Δn could enable separation of Δn and Δk.

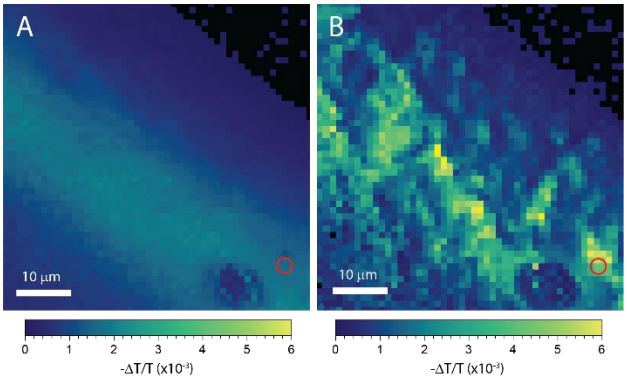

Fig. 2. Comparison of PP (A) and IPP (B) images on the same region of the porphyrin derivative thin film. Note the film edge in the upper right

corner of both images. Images were collected at a pump-probe delay time, $\Delta t_{CW} = 0\ ps$. Color scales are the same in both panels.

In Fig. 2, we compare images of a drop cast zinc-porphyrin derivative (ZnP) thin film collected using the standard pump-probe (PP) and IPP methods. To collect the images, the sample was scanned under overlapped pump and probe beams with a piezoelectric stage under identical conditions. Photoexcitation of the ZnP thin film at 400 nm (1.8 uW) produces a population of excited states, which absorb the 800 nm probe beam for $\Delta t_{CW} \geq 0\ ps$. The ground state is non-resonant with the probe ($\kappa = 0$). Comparison of the two images shows that the average signal intensity is qualitatively greater for the IPP detection than for the PP approach as expected. In addition, the images show distinct spatial differences in the optical response. Whereas the PP image shows a largely uniform response, the IPP image reveals clear structural heterogeneity in the organic film. These μm-scale variations are qualitatively consistent with similar features observed in both phase and height images collected with atomic force microscopy (SI), suggesting that they derive from local morphological or topological heterogeneity in the thin film to which standard PP microscopy is insensitive.

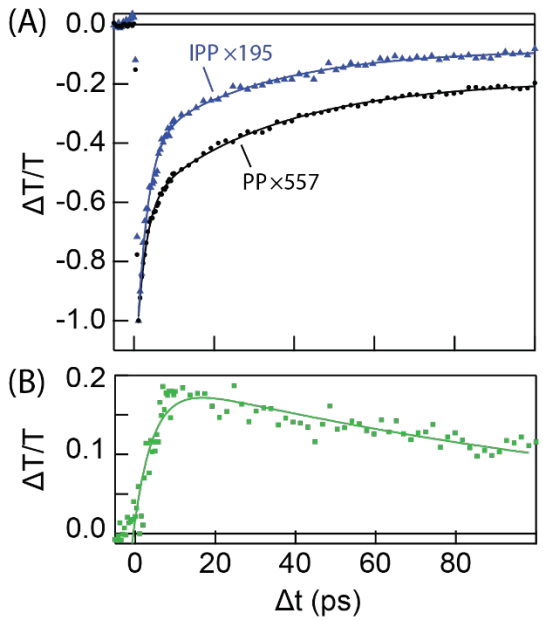

Fig. 3. (A) Comparison of kinetics traces from IPP (blue triangles) and PP (black circles) methods. Traces are normalized to the same amplitude by the indicated constant. (B) Difference between normalized kinetics in part A. The solid line shows a biexponential fit to the difference kinetics with a rise time, $\tau = 4.9$.

Fig. 3 shows a comparison between normalized IPP and PP kinetics, collected at the locations indicated by the red circles in Fig. 2A,B. At short times ($\Delta t_{CW} = 0\ ps$), the IPP signal intensity is a factor of 2.86 larger than the PP kinetics trace (note the normalization factors in panel A, whose ratio gives the enhancement factor). This signal enhancement is comparable, but slightly smaller than the factor of 3.6 expected based on the beamsplitter asymmetry, $\delta = 0.069$, assuming a purely absorptive process. A second unexpected result can be seen by comparing the kinetics traces at later times ($\Delta t_{CW} \gtrsim 5\ ps$). Here, the IPP kinetics decay more quickly than the PP kinetics. This difference in decay rate is universally observed for all regions probed on the thin film (additional location comparisons are shown in SI).

While we initially attributed the reduction in amplitude and faster decay of the IPP kinetics to contributions from the second term in Eq. 3, power dependent studies (SI) showed that both effects scale linearly with the excitation density, rather than the quadratic scaling expected from Eq. 3. The linear power scaling implicates photoinduced changes to the Fresnel coefficient at the air-thin-film interface. To account for this effect, we introduce a small pump-dependent parameter, ρ, to Eq. 1 that changes the asymmetry of the CW field, i.e. replacing δ with $\delta - \rho$. Expressing ρ in terms of Δn ,the interferometric pump probe signal, S_{IPP} , can be written as (Eq. 5, SI):

$$S_{IPP} \approx -\frac{k_0 l}{2\delta}\Delta\kappa - \frac{2}{\delta(1+n)^2}\Delta n. \qquad (5)$$

Note that in Eq. 5 the quadratic term in Δn has been dropped and the second term shows the Δn linear dependence observed experimentally.

The slightly lower than expected IPP enhancement factor at $\Delta t_{CW} = 0\ ps$ is consistent with a pump-induced reduction in the refractive index (that is $\Delta n(0\ \text{ps}) < 0$) that occurs within the time resolution of the instrument (See Eq. 5). At later times, the more quickly decaying S_{IPP} kinetics relative to S_{PP} shows that the refractive index further decreases in the first 5-10 ps after photoexcitation. Panel B of Figure 3B shows difference kinetics, $S_{PP} - S_{IPP}$, which provides a clearer perspective of these dynamics. A biexponential fit to the difference kinetics shows a rise with a time constant of $\tau = 4.9 \pm 0.4\ ps$. Both the timescale of change and the sign of Δn is consistent with pump-induced sample heating. Organic materials generally exhibit $\partial n/\partial T < 0$ due to materials expansion[19]. We attribute the 4.9 ps rise to the cooling of photogenerated excited states via phonon scattering. The resultant localized heating causes expansion, which reduces n. In contrast to the standard PP approach, interferometric detection provides excellent sensitivity to this small change in reflection.

Although the discussion outlined above suggests that comparison between PP and IPP modes can provide a means to quantify Δn and Δk, caution is necessary as small errors in δ translate to large uncertainties in the pump-induced changes to the optical constants. More robust strategies to separate absorptive and dispersive components include slight misalignment of the interferometer[20] or asymmetric placement of an active modulator in the interferometer to allow for phase shifting of the CCW beam[12, 21]. Nevertheless, as described above and is the case in many solid-state systems, even a qualitative measure of the time dependence of Δn and Δk provides insights into

excited state dynamics that are inaccessible with standard PP approaches.

Several refinements of IPP microscopy can be anticipated to expand its utility for probing a variety of materials and dynamical processes. A comparative analysis of signal to noise levels for six individual kinetics traces shows that although IPP signal magnitude is enhanced, so too is the noise, resulting in a two-fold lower S/N than PP kinetics. The enhanced noise reflects the technique's sensitivity to fluctuation in δ (SI). We expect that more robust interferometer design and environmental controls will enable S/N levels that exceed standard PP microscopy. Tracking energy and electron transport in IPP mode can be envisioned by spatially scanning the pump relative to the fixed probes[22, 23]. Reflective-mode measurements can be achieved by redesigning the interferometer, albeit with less polarization flexibility[23, 24]. Finally for characterizing high-index materials where reflected light will complicate the transmissive interferometric signal, temporal gating with a Pockels cell or acousto-optic modulator should allow separation of reflected and transmitted pulses.

In conclusion, we have demonstrated the integration of a Sagnac interferometer into a home-built pump-probe microscope operating in transmissive mode to sensitively probe excited state dynamics in an organic thin film. We show a ~3-fold increase in signal magnitude for IPP over PP measurements, limited by the balance between CW and CCW interferometer arms. IPP mode is highly sensitive to local microscale changes in the film morphology, which is likely to find particular importance in understanding structure-function relationships in organic materials. Moreover, comparisons between PP and IPP datasets, achievable by manipulating a single optical element, can provide new insight into excited state dynamics that cannot be obtained through either individual method. The ease of implementation, cost effective optics, and compatibility with various detection techniques makes IPP a compelling advancement in the capabilities of pump-probe microscopy.

Back Matter

Funding. This work supported by the National Science Foundation Award #2016360.

Acknowledgment. The authors would like to acknowledge Prof. J.H. Olivier at the University of New Mexico for providing the porphyrin derivative samples.

Disclosures. The authors declare no conflicts of interest.

Data availability. Data underlying the results presented in this paper are not publicly available at this time but may be obtained from the authors upon reasonable request.

Supplemental Document. See Supplement 1 for supporting content.

References

1. M. C. Fischer, J. W. Wilson, F. E. Robles et al., Rev Sci Instrum **87** (2016).
2. N. Gross, C. T. Kuhs, B. Ostovar et al., J Phys Chem C **127**, 14557-14586 (2023).
3. D. Davydova, A. de la Cadena, D. Akimov et al., Laser Photonics Rev **10**, 62-81 (2016).
4. Y. F. Zhu, and J. X. Cheng, J Chem Phys **152** (2020).
5. P. T. Lyu, Q. Y. Li, P. Wu et al., Journal of the American Chemical Society **144**, 13928-13937 (2022).
6. K. S. Wilson, T. S. Volek, N. Gross et al., J Phys Chem C (2024).
7. M. Liebel, F. V. A. Camargo, G. Cerullo et al., Nano Lett **21**, 1666-1671 (2021).
8. S. Adhikari, N. Gross, K. S. Wilson et al., J Phys Chem C **128**, 8708-8715 (2024).
9. M. Delor, H. L. Weaver, Q. Yu et al., Nature Materials **19**, 56-62 (2020).
10. B. Culshaw, Measurement Science and Technology **17**, R1-R16 (2006).
11. K. X. Sun, M. M. Fejer, E. Gustafson et al., Phys Rev Lett **76**, 3053-3056 (1996).
12. R. Trebino, and C. C. Hayden, Opt Lett **16**, 493-495 (1991).
13. S. Dobner, C. Cleff, C. Fallnich et al., J Chem Phys **137** (2012).
14. T. L. Courtney, S. D. Park, R. J. Hill et al., Opt. Lett. **39**, 513-516 (2014).
15. D. H. Hurley, and O. B. Wright, Opt. Lett. **24**, 1305-1307 (1999).
16. M. A. van Dijk, M. Lippitz, and M. Orrit, Physical Review Letters **95**, 267406 (2005).
17. As discussed by Trebino and Hayden in Ref. 12, an alternative configuration in which both pulses probe the pumped sample - at different delays - allows the length of the interferometer to be tuned to act as an effective high-pass filter for pump-induced transients.
18. S. C. Sheng, and A. E. Siegman, J Opt Soc Am **66**, 1032-1036 (1976).
19. P. Michel, J. Dugas, J. M. Cariou et al., J Macromol Sci Phys **B25**, 379-394 (1986).
20. K. Misawa, and T. Kobayashi, Opt Lett **20**, 1550-1552 (1995).
21. M. C. Gabriel, N. A. Whitaker, Jr., C. W. Dirk et al., Opt Lett **16**, 1334-1336 (1991).
22. N. S. Ginsberg, and W. A. Tisdale, Annu Rev Phys Chem **71**, 1-30 (2020).
23. T. Tachizaki, T. Muroya, O. Matsuda et al., Rev Sci Instrum **77** (2006).
24. H. Heo, T. Kim, Y. Jeong et al., Rev Sci Instrum **93** (2022).